The Journal of Headache and Pain

RESEARCH

Open Access

Reduced neurovascular coupling of the visual network in migraine patients with aura as revealed with arterial spin labeling MRI: is there a demand-supply mismatch behind the scenes?

Marcello Silvestro[1,2†], Fabrizio Esposito[2†], Alessandro Pasquale De Rosa[2], Ilaria Orologio[1], Francesca Trojsi[1,2], Lorenzo Tartaglione[1,2], Pablo García-Polo[3], Gioacchino Tedeschi[1,2], Alessandro Tessitore[1,2], Mario Cirillo[2] and Antonio Russo[1,2*]

Abstract

Background Although neuroimaging investigations have consistently demonstrated that "hyperresponsive" and "hyperconnected" visual cortices may represent the functional substrate of cortical spreading depolarization in patients with migraine with aura, the mechanisms which underpin the brain "tendency" to ignite the cortical spreading depolarization and, consequently, aura phenomenon are still matter of debate. Considering that triggers able to induce aura phenomenon constrain brain to increase global (such as physical activity, stressors and sleep abnormalities) or local (such as bright light visual stimulations) energy demand, a vascular supply unable to satisfy the increased energy requirement could be hypothesized in these patients.

Methods Twenty-three patients with migraine with aura, 25 patients with migraine without aura and 20 healthy controls underwent a 3-Tesla MRI study. Cerebral blood flow and local functional connectivity (regional homogeneity) maps were obtained and registered to the MNI space where 100 cortical regions were derived using a functional local-global normative parcellation. A surrogate estimate of the regional neurovascular coupling for each subject was obtained at each parcel from the correlation coefficient between the z-scored ReHo map and the z-scored cerebral blood flow maps.

Results A significantly higher regional cerebral blood flow across the visual cortex of both hemispheres (i.e. fusiform and lingual gyri) was detected in migraine with aura patients when compared to patients with migraine without aura ($p < 0.05$, corrected for multiple comparisons). Concomitantly, a significantly reduced neurovascular coupling

†Marcello Silvestro and Fabrizio Esposito contributed equally to this work.

*Correspondence:
Antonio Russo
dottor.russo@gmail.com

Full list of author information is available at the end of the article

($p < 0.05$, false discovery rate corrected) in the primary visual cortex parcel (VIS-4) of the large-scale visual network was observed in the left hemisphere of patients with migraine with aura (0.23±0.03), compared to both patients with migraine without aura (0.32±0.05) and healthy controls (0.29±0.05).

Conclusions Visual cortex neurovascular "decoupling" might represent the "link" between the exposure to trigger factors and aura phenomenon ignition. While physiological vascular oversupply may compensate neurovascular demand-supply at rest, it becomes inadequate in case of increased energy demand (e.g. when patients face with trigger factors) paving the way to the aura phenomenon ignition in patients with migraine with aura. Whether preventive treatments may exert their therapeutic activity on migraine with aura restoring the energy demands and cerebral blood flow trade-off within the visual network should be further investigated.

Keywords Migraine with aura, Arterial spin labeling, Neurovascular-coupling

Background

Migraine is a disabling disorder of brain excitability featuring episodes of headache along with sensory hypersensitivity symptoms and neurovegetative manifestations [1]. About one-third of patients experience fully reversible focal neurological symptoms encompassing the so-called migraine aura, a heterogeneous phenomenon with inter-individual and intra-individual variability [2]. In the last decades, converging advanced neuroimaging and neurophysiological evidence has strongly supported visual cortex functional changes in patients with migraine with aura (MwA) not only in the course of the aura phenomenon, suggesting its critical role in the genesis of the cortical spreading depolarization (CSD), but also during both visual and painful stimuli [3–8]. Interestingly, visual cortices have exhibited increased functional connectivity during the interictal period, implying that a "hyperconnected" visual network could be more prone to be overwhelmed by CSD [9, 10]. However, although the neural substrates of aura propagation have been rather clarified, several concerns remain regarding the neuronal mechanisms underpinning the aura ignition. Considering that aura triggers are putatively associated with increased global (such as physical activity, psychological stress and sleep pattern abnormalities) or local (i.e., occipital cortices) (such as bright light visual stimulations) cerebral energy demands [11, 12], it could be argued that a neurovascular demand-supply mismatch, unable to satisfy the increased brain energy requirement, may underpin the onset of the aura phenomenon. More specifically, while, as expected, the hyperexcitable and hyperconnected visual network is characterized by increased regional cerebral blood flow (rCBF), it is unclear whether the magnitude of compensatory hyperperfusion is sufficient to meet the increased energy requirements in patients with MwA [13]. Both neural activity and blood flow fluctuate over time during the resting-state or baseline state of the brain, (i.e., a state lacking overt sensory stimulation or a task). This baseline activity generates a tonic supply of vasodilatory signals, in the absence (or reduction) of which the nearby arteries constrict, proportionally reducing the blood flow [14]. In humans, a suitable MRI metric indexing the spatially varying coupling between local spontaneous neuronal activity and baseline rCBF would provide an operational surrogate of the regional neurovascular coupling (NVC) able to clarify the mechanisms underlying certain chronic neurological conditions [15, 16].

Herein, we hypothesize that a neurovascular demand-supply mismatch in terms of dysfunctional regional NVC of visual cortices could characterize patients with MwA, representing the substrate of brain proneness to aura ignition when functional demand increases (e.g., because of exposure to trigger factors). For this purpose, we explored the NVC within the visual network in patients with MwA compared with healthy controls (HC) to selectively explore whether **a** neurovascular demand-supply mismatch of visual cortices may characterize these patients.

To examine the specificity of any putative NVC differences between patients with MwA and HC, a group of patients with migraine without aura (MwoA) was investigated by serially acquiring multi-delay arterial spin labeling (ASL) and blood oxygen level dependent (BOLD) images at rest and combining them into a whole-cortex rCBF and regional NVC analysis, the latter obtained from the regional homogeneity (ReHo) of BOLD signals, a metric that indirectly reflects the functional integration of local spontaneous neuronal activity [17].

Patients and methods

Study population and study design

Twenty-three right-handed patients with exclusively simple visual MwA [ICHD-3 code: 1.2.1.1] according to the International Headache Society criteria (Headache Classification Subcommittee of the International Headache Society, 2018) [18], were recruited between June 2022 and March 2023 from the migraine population referring to the Headache Centre of the Department of Neurology at the University of Campania "Luigi Vanvitelli". Demographic data were obtained as well as the following clinical features: age at migraine onset, disease duration,

attacks frequency (day/month), aura duration, attacks pain intensity (assessed using numerical rating scale - NRS) and related disability (using Migraine Disability Assessment Scale -MIDAS and Headache Impact Test - HIT-6), depressive and anxious symptoms (using the Hamilton Depression Rating Scale - HDRS and Hamilton Anxiety Rating Scale -HARS). Patients with other neurological, psychiatric and internal disorders as well as pregnancy, claustrophobia and other chronic pain conditions were excluded. Twenty-five right-handed patients with episodic MwoA [ICHD-3 code: 1.1] were also recruited. Patients (and controls) were asked not to take caffeine or other stimulants on the day the scan was scheduled to be acquired. To avoid the confounding interference of migraine attack or pharmacologic intake with the fMRI findings, all patients were both headache and migraine-free and were not taking rescue medications at least 3 days before scanning. Patients were interviewed 3 days after scanning to ascertain if they were migraine-free also during the post-scan 3 days.

All patients were naïve for commonly prescribed migraine preventive medications at the time of the brain scan. Finally, twenty age- and sex-matched, right-handed subjects with less than a few spontaneous non-throbbing headaches per year, with no family history of migraine, pregnancy, claustrophobia, hypertension, diabetes mellitus, heart disease, other chronic systemic diseases, stroke, cognitive impairment, substance abuse, chronic pain, as well as other neurological or psychiatric disorders were recruited as HC. The HC recruitment was conducted via advertisements placed in the hospital (e.g. posters and flyers), word-of-mouth referrals, and from a database of research volunteers maintained by the MRI Research Centre of the University of Campania "Luigi Vanvitelli".

MRI image acquisition

MRI was performed on a 3 Tesla scanner (Discovery MR750, GE Medical Systems, Milwaukee, WI, United States) equipped with a 32-channel receive-only head–neck coil (Nova Medical, Wilmington MA, United States). For high resolution anatomical reference, the imaging protocol included a 3D T1-weighted inversion recovery fast spoiled gradient recalled echo (3D-IR-FSPGR) sequence with sagittal reconstruction (TR = 6,912 ms, IT = 650 ms, TE = 2.996 ms, flip angle = 9°, voxel size = 1×1×1 mm). For resting-state fMRI (rs-fMRI), the imaging protocol included a hyperband simultaneous multi-slice (SMS) echo-planar imaging (EPI) T2*-weighted sequence with TR = 1000 ms, TE = 30 ms, spatial resolution = 2.5×2.5×2.5 mm^3, hyperband factor = 4, acquisition matrix = 96×96, 600 dynamic volumes (total duration: 10 m 50 s), and direction of phase encoding acquisition anterior-posterior (P-A). Two additional hyperband EPI series with only 10 dynamic volumes were acquired with opposite polarity of the phase encoding direction (A-P, P-A) to be use for distortion correction of the hyperband EPI volumes of the main series. For volumetric perfusion imaging, the imaging protocol included two repetitions of a multi-delay 3D pseudo-continous arterial spin labelling (3D-pc-ASL) prototype sequence [19] with a stack of spirals readout and the following parameters: TR = 8770 ms; TE = 60.72 ms; slice thickness = 3 mm; NEX = 1; readout: 84 arms × 640 points; FOV = 220×220 mm, and reconstruction matrix = 128×128. To increase the power of the CBF estimates, while preserving an optimal compensation of arterial transit time (ATT) variability across subjects, each ASL scan encoded seven images with two different sets of post-labeling delay (PLD) times and one reference (M0) image into a single series. In the first ASL scan, PLD times were spaced exponentially (700, 905, 1138, 1411, 1737, 2145 and 2687 ms) resulting in variable effective label durations (205, 234, 272, 327, 407, 542 and 813 ms). In the second ASL scan, PLD were space linearly (700, 1100, 1500, 1900, 2300, 2700, 3100 ms) resulting in constant effective LDs (400 ms). Each ASL scan lasted 10 min and 52 s. During the entire acquisition, all subjects wore headphones and were instructed to lie still in a supine position and to stay awake with their eyes closed.

ASL MRI data preprocessing

3D ASL time-series were preprocessed with BASIL [20], a tool from the FMRIB Software Library (FSL) (https://fsl.fmrib.ox.ac.uk/fsl/fslwiki/). The CBF maps were obtained by applying the kinetic model inversion with voxel-wise calibration using the M0 image and all the pairs of PLD/LD values specified in each ASL acquisition (with exponential and linear PLD/LD distribution). The correction for arterial transit time (ATT) was obtained by taking the mean of the estimated CBF across all PLD/LD pairs. To also mitigate the impact of the partial volume effect (PVE), the spatially regularized kinetic curve model was applied by providing the tissue probability maps for white and grey matter as resulting from the multi-class segmentation of the 3D-T1w images performed with SPM12 [21] (www.fil.ion.ucl.ac.uk/spm/). The calibrated (ATT- and PVE-corrected) CBF maps were finally normalized to the Montreal Neurological Institute (MNI) standard template using the transformation resulting from the DARTEL workflow after co-registration of the M0 images to the 3D T1-weighted images.

fMRI image data preprocessing

Susceptibility distortion correction of rs-fMRI images was performed with FSL 6.0.4 [22]. The corrected volumes were then entered into the fMRIPrep pipeline (v22.1.1) where the following steps were applied: skull

stripping, motion correction, slice-time correction, co-registration to the 3D-T1w scan, physiological confound estimation [23]. In order to reduce the residuals of head motion and physiological noise, 24 motion-related predictors (6 head motion parameter time-series, their first-order derivatives, and the 12 corresponding squared parameter time-series) and the mean time-courses from the white matter mask and the cerebrospinal fluid mask (as obtained from fMRIPrep anatomical preprocessing) were regressed out from the data [24]. An additional spike-related regressor was created to account for residual motion-related spikes. This regressor was derived from the framewise displacement (FD) time-series, with a value of 1 at the time points of each detected spike (i.e., FD > 0.5 mm) and a value of 0 elsewhere. The image time-series were finally band-pass filtered between 0.01 Hz and 0.1 Hz and regional homogeneity (ReHo) maps were calculated using the Kendall's coefficient concordance (KCC) [25]. KCC measures the local synchronization between the time-course at each voxel and time-courses at its nearest 26 neighboring voxels. ReHo maps were computed in the native space of EPI series and spatially normalized with SPM12 to the MNI standard template using the DARTEL approach, after co-registration to the T1w images [26].

ASL MRI image data preprocessing

For each subject and each scan, the mean CBF across all gray matter voxels was calculated thus providing an estimate for the global CBF (gCBF). The two independent CBF estimates resulting from the two ASL scans (with exponential and linear PLDs) were treated as two repeated observations for gCBF as well as the CBF at each voxel. The (MNI-normalized) CBF maps were also transformed to Z-score maps by subtracting the global mean (gCBF) and dividing by the standard deviation across all voxels. The Z-scored rCBF maps were then spatially smoothed with an isotropic gaussian kernel (FWHM 6 mm) and the two repetitions averaged at each voxel.

MRI image data analysis

Voxel-based between-group comparisons of rCBF and ReHo maps were performed over the whole cerebral cortex. For these comparisons, a general linear model (GLM) was set-up using the GLM design builder of the FMRIB Software Library (FSL) (https://fsl.fmrib.ox.ac.uk/fsl/docs/#/). The design matrix included three columns for group membership specification (MwoA, MwA, HC) and three more columns for confounding effects (age, sex, frequency of migraine attacks). For non-parametric inference, the FSL tool "randomize" [27] was used to compute t-statistics maps for the following differential contrasts: "MwA vs. MwoA", "MwA vs. HC" and "MwoA vs. HC". Threshold-free cluster enhancement (TFCE) was used to detect clusters with statistically significant effects ($p < 0.05$) with correction for multiple voxel-level comparisons. For image display purposes, the resulting volumetric contrast maps were imported to the software package BrainVoyager (www.brainvoyager.com) and here projected from the volume to the surface mesh reconstruction of the two cortical hemispheres as obtained from the segmentation of a high resolution version of the MNI T1-weighted template.

Neurovascular-coupling (NVC) data analysis

As both CBF and ReHo maps were ultimately registered to the MNI space, one hundred bilateral cortical regions were derived on the MNI template using the functional local-global parcellation introduced by Schaefer et al. [28]. This parcellation reflects the maximal ReHo of rs-fMRI signals across the cerebral cortex in a large normative population and besides it allows linking any of its cortical parcels to one of the 7 canonical large-scale resting-state functional networks [29]. Thus, we applied this cortical parcellation to both rCBF and ReHo normalized maps. In this way, a surrogate estimate for the NVC for each subject could be obtained by calculating the correlation coefficient between the z-scored ReHo map and the z-scored CBF maps, both across all gray matter voxels, thus resulting in an estimate for the global NVC (gNVC), and across all voxels of any selected cortical parcel, thus resulting in an estimate for the regional NVC (rNVC) [30]. As we are interested in obtaining the rNVC estimate within cortical regions of the visual network, we obtained an estimate for both the (absolute) rCBF and the rNVC in each experimental group, after correcting individual values for age, sex and global values (gCBF, gNVC) using linear regression. For all such parcels (VIS-X), to avoid biases because of the small sample size, we performed group statistical comparisons on the adjusted NVC estimates using the Kruskal-Wallis test (for all three groups) and the rank-sum test (for two groups). The resulting p-values were corrected for the number of performed comparisons via the False Discovery Rate (FDR) [31].

Statistical analysis

The sample size was calculated by means of G*Power software developed by the University of Dusseldorf (version 3.1.9.7), setting a conventional level for the type I error probability (alpha = 5%) for the estimation of effects sought (by both as differences between the mean of the measurements in patients and controls and as a correlation between individual measures and intensity of migraine attacks in patients), assuming independent samples and a normal distribution of the statistical parameter in the populations studied. From these analyses, it emerged that a whole sample of 48 patients with MwA

Table 1 Demographic and clinical features of patients with MwA, patients with MwoA and HC

Parameter	Group	Median ± IQ	*p* value
Gender	MwA	6 M; 17 F	-
	MwoA	10 M; 15 F	
	HC	7 M; 13 F	
Age (years)	MwA	29 ± 12	0.901
	MwoA	28 ± 10	
	HC	28 ± 4.17	
Frequency (attacks/month)	MwA	2 ± 3.5	***0.012***
	MwoA	6 ± 6	
Duration of attacks (hours)	MwA	5 ± 7	0.093
	MwoA	12 ± 22	
Duration of aura (minutes)	MwA	20 ± 15	-
Time since last headache attack to the scan (days)	MwA	11.7 ± 5.6	< 0.01
	MwoA	6.4 ± 2.3	
NRS	MwA	8 ± 1	0.298
	MwoA	8 ± 1	
MIDAS	MwA	10 ± 20	0.624
	MwoA	10 ± 21	
HIT-6	MwA	60 ± 13	0.120
	MwoA	62 ± 10	
HARS	MwA	6 ± 9	0.553
	MwoA	6 ± 9	
	HC	6 ± 6	
HDRS	MwA	7 ± 9	0.118
	MwoA	9 ± 7	
	HC	5 ± 4.5	

MwA: migraine with aura; MwoA: migraine without aura; HC: healthy controls; IQ: interquartile range; M: male; F: female; NRS: numerical rating scale; MIDAS: migraine disability assessment scale; HIT-6: headache impact test-6; HARS: Hamilton anxiety rating scale; HDRS: Hamilton depression rating scale

and MwoA ensures a statistical power of 95% taking as reference the possible alterations of the resting-state fMRI activity of the visual network as reported in our previous study in terms of z-scores of the visual component (patients with MwA: 2.31 ± 0.4; patients with MwoA: 0.91 ± 0.2; HC: 0.92 ± 0.2) [9]. For the analysis of differences among groups on demographic and clinical variables we used nonparametric tests (Kruskal-Wallis H test to compare 3 samples and the Mann-Whitney U test to compare 2 samples) to avoid biases because of the small sample size. Hypothesis testing was 2-tailed and results have been considered statistically significant if $p < 0.05$. Within the sample of patients with MwA, the correlation analysis between the imaging and clinical parameters of disease severity was carried out by means of Spearman's rank correlation coefficient. Although a p value < 0.05 was considered statistically significant, the Bonferroni correction for multiple comparisons was applied.

Finally, a logistic regression analysis has been conducted to ascertain whether rCBF and NVC changes in visual areas (considered as continuous variables) were able to discriminate patients with MwA from patients with MwoA. The ROC curve has been calculated using the "lroc" command of STATA (ROC curve after logistic regression) which, regardless of how many predictors are in the logistic model, calculates the ROC curve using the predicted probability generated by the model as the varying parameter. All statistics were performed using STATA version 16 and Statistical Package for Social Science version 20 (SPSS, Chicago, IL).

Table 2 Logistic regression analyses assessing capability of CBF changes and neurovascular-coupling abnormalities to discriminate between patients with MwA and patients with MwoA

Variable	Beta [CI 95%]	*p*-value	SE
Simple Regression			
Left fusiform gyrus rCBF	−0.03 [−0.19, 0.13]	0.716	0.08
Left lingual gyrus rCBF	0.10 [−0.05, 0.26]	0.183	0.08
Right fusiform gyrus rCBF	0.18 [−0.00, 0.36]	***0.049***	0.09
Right lingual gyrus rCBF	−0.06 [−0.23, 0.12]	*0.529*	0.09
Left VIS-4 neurovascular coupling	−9.55 [-18.65, -0.45]	**0.040**	4.64
Left VIS-5 neurovascular coupling	-4.03 [-10.84, 2.79]	0.247	3.48

Model LR χ^2 (2) = 23.08; p-value = 0.0008; pseudo R^2 = 0.26 (Nagelkerke)

SE: Standard Error; rCBF: regional cerebral blood flow;

Results

Clinical findings

The three experimental groups (i.e., MwA, MwoA and HC) did not differ in age and male/female ratio. Similarly, no differences were observed in clinical parameters of migraine severity (disease duration, average of pain intensity of migraine attacks, MIDAS, HIT-6) and comorbid anxious and depressive symptoms (HARS and HDRS) except for the frequency of attacks (attacks/year) which, as expected [32–34], was significantly lower in patients with MwA compared to patients with MwoA (See Table 1).

Multi delay-3D-pc-ASL

CBF and ReHo analysis

The voxel-based CBF analysis over the entire cerebral cortex revealed four clusters with statistically significant differences encompassing different cortical parcels between experimental groups (Fig. 1). When compared to patients with MwoA, patients with MwA showed a higher CBF ($p < 0.05$, TFCE corrected) in the occipital cortex, along the lingual and fusiform gyri of both hemispheres, encompassing the fourth (VIS-4) and fifth (VIS-5) cortical parcels of the visual network. When compared with HC, patients with MwoA showed an increased rCBF ($P < 0.05$, TFCE corrected) in the right pre-supplementary motor area, encompassing the second cortical parcel of the salience ventro-medial attention network (R-SVAN-M2), and in the right middle frontal gyrus, encompassing

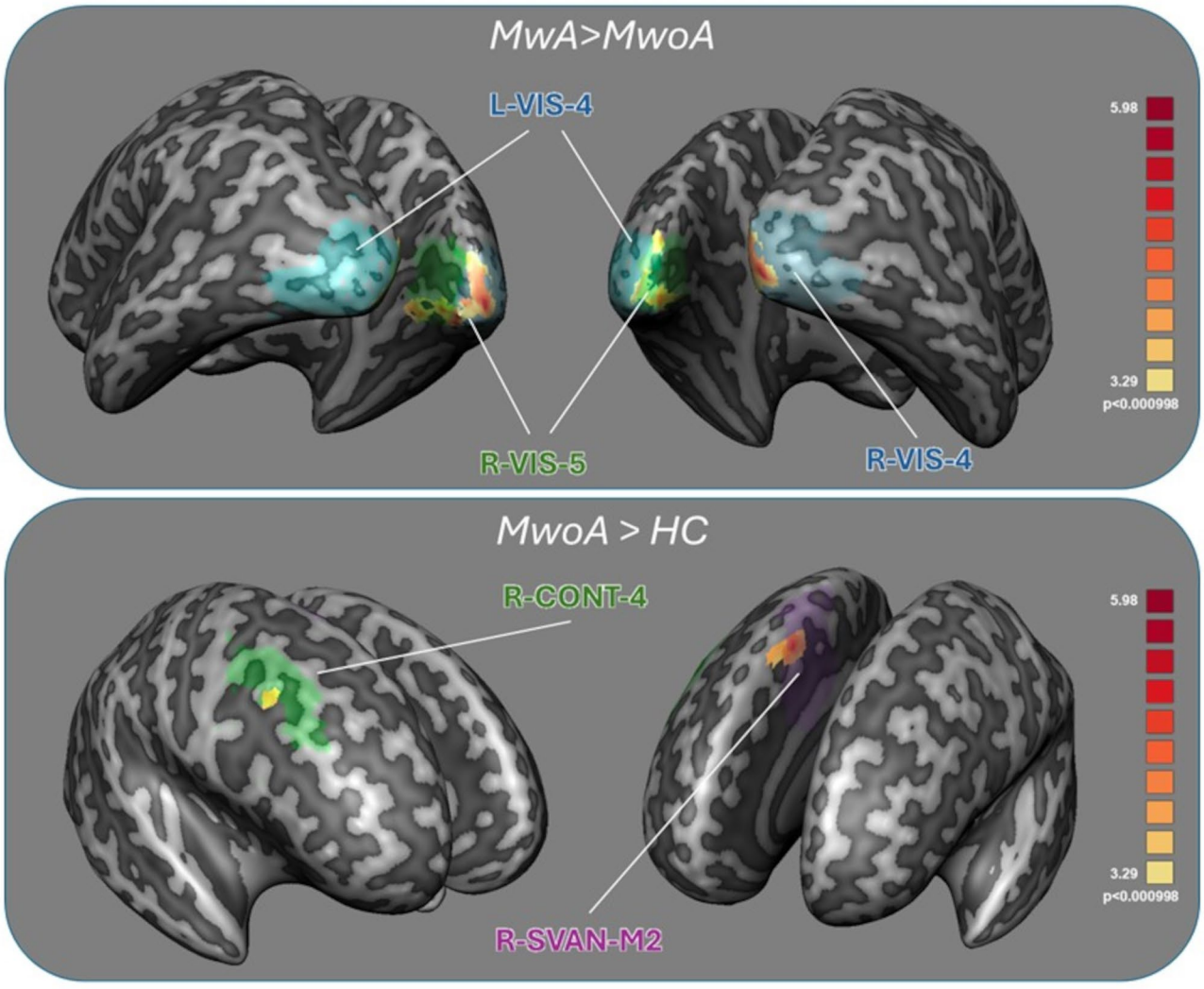

Fig. 1 Significant differences in voxel-based CBF maps ($p < 0.05$ – TFCE corrected) between MwA and MwoA patients (up) and MwoA and HC (down). Clusters with significant effects are displayed and labelled on cortical parcels (according to Schaefer atlas) of the cortical surface mesh reconstructed from the MNI template brain. CBF: cerebral blood flow; TFCE: threshold-free cluster-enhancement; MwA: migraine with aura; MwoA: migraine without aura; HC: healthy controls; VIS-4, VIS-5: parcels from the visual network; CONT-4: parcel from the executive control network; SVAN-M: parcel from the salience ventral medial attention network

the fourth cortical parcel of the dorso-lateral executive control network (R-CONT-4). There were no clusters with significant rCBF differences between patients with MwA and HC at the same statistical threshold.

The voxel-based ReHo analysis over the entire cerebral cortex revealed no clusters with significant ReHo differences between the experimental groups.

NVC analysis

When applying the cortical parcellation to both CBF and ReHo normalized maps, and assessing NVC across all parcels of the visual network, we found a significantly reduced ($p < 0.05$, FDR = 0.049) NVC for the VIS-4 parcel of the left occipital cortex in patients with MwA, compared to both patients with MwoA ($p = 0.001$) and HC ($p = 0.016$) but not in patients with MwoA compared to HC ($p = 0.52$) (Fig. 2). Similar tendencies were noted for the VIS-5 parcel (MwA vs. MwoA: $p = 0.027$, MwA vs. HC: $p = 0.008$) but these effects did not reach the level for FDR correction (FDR = 0.11) (Fig. 2).

Correlation analysis and logistic regression analysis

We found no correlations between rCBF or NVC and both demographic data and clinical parameters of disease severity (disease duration, migraine attacks frequency, duration, and pain intensity, MIDAS and HIT-6 scores). The logistic regression analysis showed that a model considering the rCBF from right and left lingual and fusiform giri and NVC for VIS-4 and VIS-5 parcels (from Schaefer atlas) significantly and acceptably discriminates patients

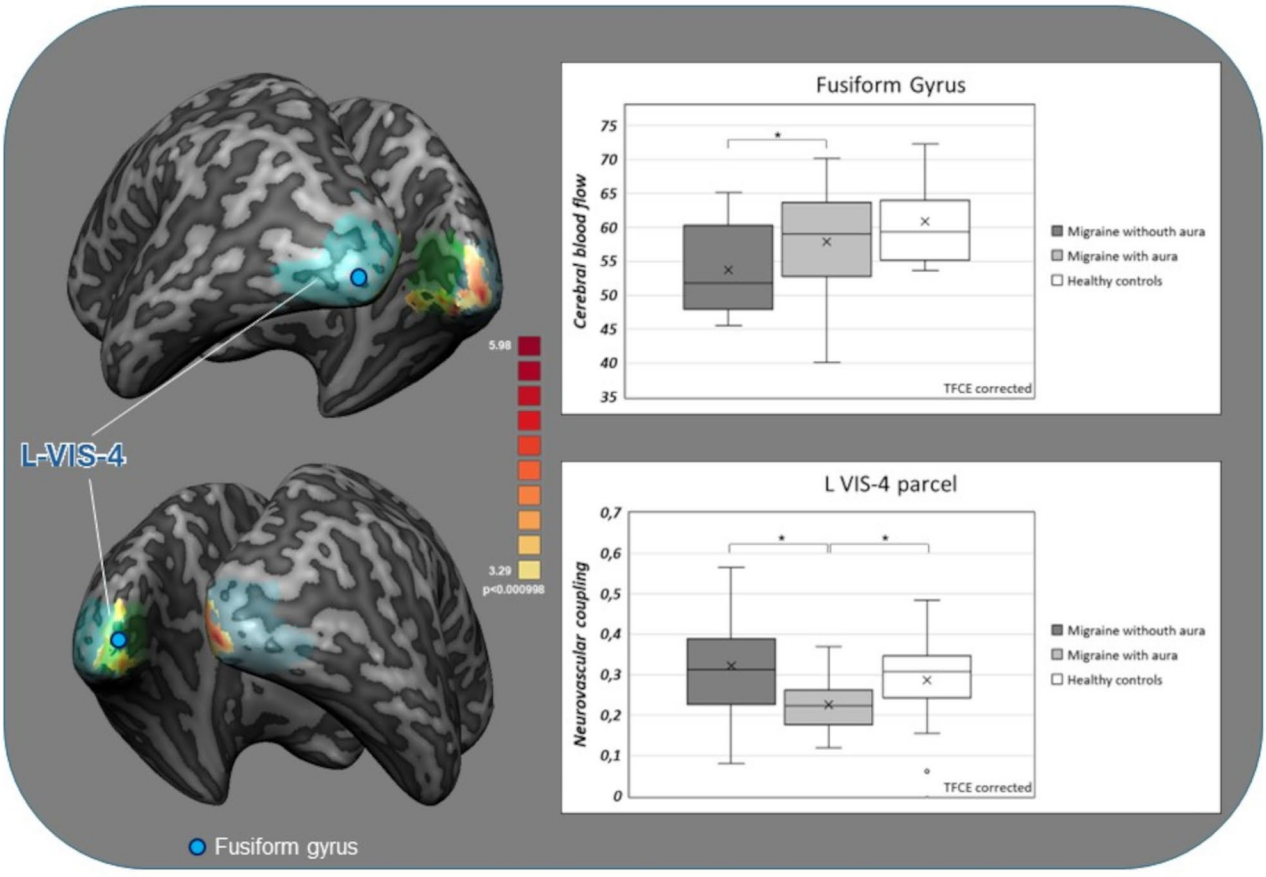

Fig. 2 Significant differences in visual areas voxel-based CBF maps and VIS-4 parcel neurovascular-coupling according to Schaefer atlas (TFCE corrected) showed on inflated brains; Box-plots of in patients with MwA, patients with MwoA and HC. * $p < 0.05$ TFCE corrected. CBF: cerebral blood flow; VIS-4: parcel from the visual network; TFCE: threshold free cluster enhancement; MwA: migraine with aura; MwoA: migraine without aura; HC: healthy controls

with MwA from patients with MwoA (See Table 2). Specifically, the logistic regression model was statistically significant, likelihood ratio $\chi2(2)=23.08$, $p=0.0008$. The model explained 34.7% (Nagelkerke R2) of the variance and correctly classified 87% of patients (i.e. patients with MwA and patients with MwoA). Analysis of coefficients demonstrated that right fusiform gyrus rCBF and L-VIS-4 parcel NVC were associated with an increased likelihood of exhibiting MwA (respectively beta coefficient 0.18 $p=0.049$ and beta coefficient: -9.55, $p=0.040$) (Table 2). ROC curves showed AUC=0.87 for the full model (See Figure 3).

Discussion

In the present study, we demonstrate a reduced NVC of the visual network in patients with MwA, (explored during the interictal period) when compared to patients with MwoA and HC.

In the last decades, advanced neuroimaging and neurophysiological investigations have consistently demonstrated functional abnormalities within the extrastriate cortex, both during ictal and interictal periods, a strategic hub within the visual network, widely considered to be involved in the genesis of the "CSD", the neurophysiological process underpinning migraine aura [3–10, 35–37]. While increased resting functional connectivity and responsiveness could make visual areas more prone to be overwhelmed by the CSD propagation [10], the mechanisms underpinning the proneness to CSD ignition are still matter of debate [9]. Therefore, it could be arguable that also an increased rCBF at rest could characterize visual areas of patients with MwA [13]. Indeed, according to the physiological concept of "functional hyperemia", increased neural activity is accompanied by the local dilation of arterioles and micro-vessels to supply local blood flow and volume, and oxygenation [38]. More in depth, "functional hyperemia" is part of a more complex biological process – the so-called NVC - aimed to govern the mutual relationship between neuronal activity demand and perfusion supply [39]. The neuronal energy demands at rest are physiologically oversupplied so that further increase of rCBF is not always required to support an increased neuronal activity.

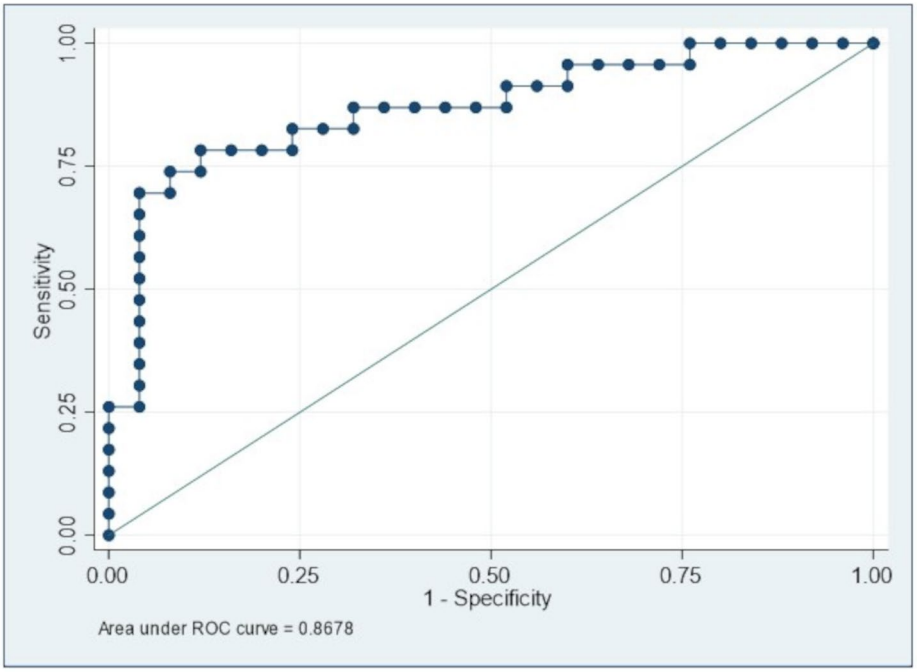

Fig. 3 ROC curve analysis of logistic regression model to classify MwA and MwoA patients considering the rCBF of primary and secondary visual cortices and neurovascular-coupling of L-VIS-4 and L-VIS-5 parcel from Schaefer atlas. MwA: migraine with aura; MwoA: migraine without aura; rCBF: regional cerebral blood flow; VIS-4 and VIS-5: parcels from the visual network

The rCBF physiological oversupply is the reason why, despite the observed NVC reduction in patients with MwA, it remains sufficient to support the hyperresponsive and hyperconnected visual cortices in these patients [40]. However, we speculate that when patients with MwA face with experience associated with an increased energy demand (as putatively happens when they come across trigger factors, such as bright or flickering lights, sleep deprivation, or physical exercise) the physiological rCBF oversupply may become inadequate [12].

In other words, the reduced NVC characterizing the visual network in patients with MwA might represent the link between the ignition of the aura phenomenon and the exposure to the trigger factors. It is important to note that while regional NVC is estimated by correlating ReHo and CBF maps within the same region, the regional CBF is obtained from the average of CBF across all voxels of the region. In other words, when calculating the NVC, both ReHo and CBF maps are converted to regional z-scores, thereby any possible bias of the regional CBF (as well as the regional ReHo) is removed as NVC should only quantify whether (and to what extent) the spatial change in two measures is more (or less) coupled within the region.

This is in line also with recent findings from provocative studies showing that in about 40% of patients with migraine with aura intravenous infusion of CGRP is able to induce migraine aura although, due to its size, CGRP is unable to pass through the blood-brain barrier [41]. Indeed, it has been suggested that CGRP-induced vasodilation may mechanically stimulate perivascular primary afferents, leading to the transmission of nociceptive information to the brain cortex through second-order and third-order neurons [42] able to provide sufficient excitatory stimuli to brain areas such as the visual cortex, lowering, in turn, the threshold for CSD initiation in "predisposed" patients [8, 43]. Our present arterial spin labeling findings suggest that a reduced NVC may properly represent the evoked MwA "predisposition".

The present findings are in agreement also with observations showing that hypoxia, a trigger factor capable of ignite aura phenomenon in patients with MwA, is able to induce, despite the hypoxia-related increase in rCBF, an abnormal increase in the lactate concentration of the visual cortex, suggesting a metabolic uncoupling in terms of an increment of blood flow not adequate to support the escalating energy demand in these patients [44].

Intriguingly, although further observations are warranted, also the patent foramen ovale, frequently found as a MwA comorbidity, could affect NVC, likely due to microembolism-related occipital cortex hyperexcitability [45].

Moreover, in support to the suggested pathophysiological model, interventions capable of suppressing primary visual cortex hyperresponsiveness to specific visual stimuli (i.e. shielding light lenses) [37] as well as preventive

pharmacological therapies such as lamotrigine and topiramate (by inhibiting the occipital cortical hyperexcitability to visual stimuli probably enhancing GABA and reducing glutamate levels) [6, 46, 47] result in a reduced frequency of migraine attacks. More in depth, it could be argued that the effects of such antiepileptic drugs in the prevention of MwA attacks can be achieved by restoring the demand-supply mismatch between brain energy demands and rCBF (that is nothing other than "NVC") within the visual network [48].

It is noteworthy that logistic regression analysis has shown that the full model, considering rCBF in VIS-4 and VIS-5 and NVC in the VIS-4 parcel from the Schaefer atlas, can discriminate MwA patients from MwoA (AUC=0.87). Moreover, as demonstrated by the analysis of the coefficient, the VIS-5 rCBF and, above all, the VIS-4 NVC were associated with a significantly increased likelihood of experiencing an aura phenomenon.

It is important to remark that higher CBF values in visual cortical areas were here found only in MwA compared to MwoA patients, whereas the same differences were not identically found between MwA patients and controls. Therefore, future ASL MRI studies are needed to accurately reproduce more general CBF findings concerning MwA and MwoA patients in comparison to HC. Nonetheless, although the aim of the study was to investigate putative NVC abnormalities in the visual network in patients with MwA, rCBF abnormalities were also detected in patients with MwoA across two different large-scale brain networks, in comparison to HC. Particularly, the increased rCBF within the salience and executive networks in patients with MwoA compared with HC, might indicate the involvement of these large-scale networks in the detection and integration of emotional and sensory stimuli, as well as in the control of externally directed attention [49]. Interictal dysfunction of these networks may contribute to the dysregulation of emotional and cognitive functions sometimes observed in migraine as well as to the different susceptibility to migraine attacks along with the transition from interictal to ictal states [50].

The present study is not exempt from limitations. First, although calculating the local spatial correlation between rCBF and ReHo maps represents a straightforward approach to capture the relationship between local neural activity and blood flow [51–53], further exploration is mandatory as happens with all current MRI methods estimating NVC, to date. Second, in the present study we used ReHo for the NVC estimate, which primarily index the local input and processing of neuronal information within functional parcels. Thereby, assuming that higher or lower similarities of one voxel with the surrounding voxels are also affected by the amount of neurovascular coupling around that voxel itself, the resulting spatial correlation between ReHo and CBF distributions should provide a suitable metric for the region-specific neurovascular coupling.

Third, both signal-to-noise and spatio-temporal resolution are higher for fMRI, compared to ASL images and this is the reason why we did not derive voxel-based estimates for NVC (e.g., as a CBF/ReHo ratio). However, the registration of the images to a common brain space at a higher (isotropic) spatial resolution (2 mm), together with the partial volume correction and the region-specific estimation based on a functionally stable parcellation, provides a reasonable technical solution to address the issue, mitigating the impact of the spatial mismatch between two modalities.

Fourth, our interpretations assume that neurovascular "decoupling", underlying aura phenomenon ignition, is triggered by experience able to increase brain energy demand, such as intense light stimulation, physical activity, or alterations in the sleep-wake rhythm. Although these trigger factors are extensively reported by a significant percentage of patients [12] they are not consistently confirmed in provocative studies [11], suggesting either a putative recall bias in patients' reports or, more likely, the difference between experimental settings and ecological systems being the "brain predisposition to migraine/aura" ignition due to maladaptive changes of brain function closely related to incremental allostatic load [54] where the relative contribution of each "effector" is unknown but seems to be additive or cumulative over time [55].

On the other hand, homogeneity of the patients' sample still represents a strength of the present study, also considering the rarity of patients experiencing exclusively migraine with visual aura.

Conclusion

Reduced NVC in the visual network centered on the VIS-4 parcel may represent the link between the ignition of the aura phenomenon and exposure to trigger factors characterizing patients with MwA. Future longitudinal investigations are needed to confirm the present findings in a larger sample of patients with MwA and to clarify whether the effectiveness of preventive treatment on MwA attack frequency implies a remodulation (and normalization) of NVC within the visual areas in these patients.

Abbreviations

3D-IR-FSPGR	3D T1-weighted inversion recovery fast spoiled gradient recalled echo
3D- pc-ASL	3D pseudo-continous arterial spin labelling
A-P	anterior-posterior
ATT	arterial transit time
BOLD	blood oxygen level dependent
CBF	cerebral blood flow
CONT-4	dorso-lateral executive control network
CSD	cortical spreading depolarization
EPI	echo-planar imaging

FD	framewise displacement
gCBF	global cerebral blood flow
gNVC	global neurovascular-coupling
HARS	Hamilton Anxiety Rating Scale
HDRS	Hamilton Depression Rating Scale
HC	healthy controls
HIT-6	Headache Impact Test
KCC	Kendall's coefficient concordance
MIDAS	Migraine Disability Assessment Scale
MNI	Montreal Neurological Institute
MwA	migraine with aura
MwoA	migraine without aura
NRS	numerical rating scale
NVC	neurovascular-coupling
PFO	patent foramen ovale
PLD	post-labeling delay
PVE	partial volume effect
rCBF	regional cerebral blood flow
ReHo	regional homogeneity
rNVC	regional neurovascular-coupling
rs-fMRI	resting-state fMRI
SMS	simultaneous multi-slice
SN	salience network
SPSS	Statistical Package for Social Science
SVAN-M2	salience ventro-medial attention network
TFCE	threshold-free cluster enhancement

Acknowledgements
Not applicable.

Author contributions
M.S. literature review, experimental design, image data analysis, results interpretation, manuscript drafting. F.E. Literature review, experimental design, image data analysis, results interpretation, manuscript drafting and revision. ADR Data analysis, manuscript drafting. I.O. Experimental design, results interpretation, manuscript revision. F.T. Literature review and results interpretation. L.T. Image data acquisition. P.G.P. Image data acquisition. G.T. Experimental design, results interpretation, manuscript revision. A.T. Data analysis, manuscript drafting and revision. M.C. Image data analysis and results interpretation. A.R. Literature review, experimental design, image data analysis, results interpretation, manuscript drafting and revision.

Funding
Work supported by #NEXTGENERATIONEU (NGEU) and funded by the Ministry of University and Research (MUR), National Recovery and Resilience Plan (NRRP), project MNESYS (PE0000006) – A Multiscale integrated approach to the study of the nervous system in health and disease (DN. 1553 11.10.2022).

Data availability
All data generated or analysed during this study are available upon reasonable request from the corresponding author (dottor.russo@gmail.com).

Declarations

Ethics approval and consent to participate
The study was approved by the Ethics Committee of University of Campania "Luigi Vanvitelli" with protocol number 0013971, and written informed consent was obtained from all subjects according to the Declaration of Helsinki.

Consent for publication
Not applicable.

Competing interests
The author(s) declared the following potential conflicts of interest with respect to the research, authorship, and/or publication of this article:
Dr Silvestro has received speaker honoraria from Novartis, Teva and Lilly.
Professor Tessitore has received speaker honoraria from Novartis, Schwarz Pharma/UCB, Lundbeck, Abbvie and Glaxo.
Professor Tedeschi has received speaker honoraria from Sanofi-Aventis, Merck Serono, Bayer Schering Pharma, Novartis, Biogen-Dompe´ AG, Teva and Lilly; has received funding for travel from Bayer Schering Pharma, Biogen-Dompe´ AG, Merck Serono, Novartis and Sanofi Aventis; and serves as an associate editor of Neurological Sciences.
Professor Russo has received speaker honoraria from Allergan, Lilly, Pfizer, Novartis and Teva and serves as an associate editor of Frontiers in Neurology (Headache Medicine and Facial Pain session).
The other authors have nothing to declare.

Author details
[1]Headache Centre, Department of Advanced Medical and Surgical Sciences, University of Campania "Luigi Vanvitelli", Naples, Italy
[2]Advanced MRI Neuroimaging Centre, Department of Advanced Medical and Surgical Sciences, University of Campania "Luigi Vanvitelli", Naples, Italy
[3]General Electric Healthcare, Madrid, Spain

Received: 3 April 2024 / Accepted: 4 October 2024
Published online: 15 October 2024

References

1. Noseda R, Burstein R (2013) Migraine pathophysiology: anatomy of the trigeminovascular pathway and associated neurological symptoms, cortical spreading depression, sensitization, and modulation of pain. Pain 154(Suppl 1):S44–S53
2. Viana M, Sances G, Linde M et al (2017) Clinical features of migraine aura: results from a prospective diary-aided study. Cephalalgia 37(10):979–989
3. Russo A, Silvestro M, Tessitore A, Tedeschi G (2019) Recent insights in Migraine with Aura: a narrative review of Advanced Neuroimaging. Headache 59(4):637–649
4. Aurora SK, Cao Y, Bowyer SM, Welch KM (1999) The occipital cortex is hyperexcitable in migraine: experimental evidence. Headache 39(7):469–476
5. Hadjikhani N, Del Rio S, Wu M, O. et al (2001) Mechanisms of migraine aura revealed by functional MRI in human visual cortex. Proc Natl Acad Sci USA 98(8):4687–4692
6. Cao Y, Welch KM, Aurora S, Vikingstad EM (1999) Functional MRI-BOLD of visually triggered headache in patients with migraine. Arch Neurol 56(5):548–554
7. Datta R, Aguirre GK, Hu S, Detre JA, Cucchiara B (2013) Interictal cortical hyperresponsiveness in migraine is directly related to the presence of aura. Cephalalgia 33(6):365–374
8. Russo A, Tessitore A, Silvestro M et al (2019) Advanced visual network and cerebellar hyperresponsiveness to trigeminal nociception in migraine with aura. J Headache Pain 20(1):46
9. Tedeschi G, Russo A, Conte F et al (2016) Increased interictal visual network connectivity in patients with migraine with aura. Cephalalgia 36(2):139–147
10. Vinogradova LV (2018) Initiation of spreading depression by synaptic and network hyperactivity: insights into trigger mechanisms of migraine aura. Cephalalgia 38(6):1177–1187
11. Hougaard A, Amin FM, Hauge AW, Ashina M, Olesen J (2013) Provocation of migraine with aura using natural trigger factors. Neurology 80(5):428–431
12. Lindblad M, Hougaard A, Amin FM, Ashina M (2017) Can migraine aura be provoked experimentally? A systematic review of potential methods for the provocation of migraine aura. Cephalalgia 37(1):74–88
13. Michels L, Villanueva J, O'Gorman R et al (2019) Interictal Hyperperfusion in the higher visual cortex in patients with episodic migraine. Headache 59(10):1808–1820
14. Echagarruga CT, Gheres KW, Norwood JN, Drew PJ (2020) nNOS-expressing interneurons control basal and behaviorally evoked arterial dilation in somatosensory cortex of mice. eLife, 9, e60533
15. Phillips AA, Chan FH, Zheng MM, Krassioukov AV, Ainslie PN (2016) Neurovascular coupling in humans: physiology, methodological advances and clinical implications. J Cereb Blood Flow Metab 36(4):647–664
16. Drew PJ (2022) Neurovascular coupling: motive unknown. Trends Neurosci 45(11):809–819
17. Zhang Y, Zhang X, Ma G, Qin W, Yang J, Lin J, Zhang Q (2021) Neurovascular coupling alterations in type 2 diabetes: a 5-year longitudinal MRI study. BMJ open Diabetes Res Care, 9(1), e001433
18. Headache Classification Committee of the International Headache Society (IHS) The International Classification of Headache Disorders, 3rd edition (2018) Cephalalgia, 38(1), 1–211
19. Alsop DC, Detre JA, Golay X et al (2015) Recommended implementation of arterial spin-labeled perfusion MRI for clinical applications: a consensus of

the ISMRM perfusion study group and the European consortium for ASL in dementia. Magn Reson Med 73(1):102–116
20. Groves AR, Chappell MA, Woolrich MW (2009) Combined spatial and non-spatial prior for inference on MRI time-series. NeuroImage 45(3):795–809
21. Chappell MA, Groves AR, MacIntosh BJ, Donahue MJ, Jezzard P, Woolrich MW (2011) Partial volume correction of multiple inversion time arterial spin labeling MRI data. Magn Reson Med 65(4):1173–1183
22. Smith SM, Jenkinson M, Woolrich MW et al (2004) Advances in functional and structural MR image analysis and implementation as FSL. NeuroImage 23(Suppl 1):S208–S219
23. Esteban O, Markiewicz CJ, Blair RW et al (2019) fMRIPrep: a robust preprocessing pipeline for functional MRI. Nat Methods 16(1):111–116
24. Friston KJ, Williams S, Howard R, Frackowiak RS, Turner R (1996) Movement-related effects in fMRI time-series. Magn Reson Med 35(3):346–355
25. Zang Y, Jiang T, Lu Y, He Y, Tian L (2004) Regional homogeneity approach to fMRI data analysis. NeuroImage 22(1):394–400
26. Ashburner J (2007) A fast diffeomorphic image registration algorithm. NeuroImage 38(1):95–113
27. Winkler AM, Ridgway GR, Webster MA, Smith SM, Nichols TE (2014) Permutation inference for the general linear model. NeuroImage 92(100):381–397
28. Schaefer A, Kong R, Gordon EM et al (2018) Local-global parcellation of the Human Cerebral Cortex from intrinsic functional connectivity MRI. Cereb Cortex 28(9):3095–3114
29. Yeo BT, Krienen FM, Sepulcre J et al (2011) The organization of the human cerebral cortex estimated by intrinsic functional connectivity. J Neurophysiol 106(3):1125–1165
30. Guo X, Zhu J, Zhang N et al (2019) Altered neurovascular coupling in neuromyelitis optica. Hum Brain Mapp 40(3):976–986
31. Benjamini Y, Hochberg Y (1995) Controlling the false Discovery rate: a practical and powerful Approach to multiple testing. J R Stat Soc Ser B Stat Methodol 57(1):289–300
32. Lipton RB, Bigal ME, Diamond M, Freitag F, Reed ML, Stewart WF, AMPP Advisory Group (2007) Migraine prevalence, disease burden, and the need for preventive therapy. Neurology 68(5):343–349
33. Eriksen MK, Thomsen LL, Andersen I, Nazim F, Olesen J (2004) Clinical characteristics of 362 patients with familial migraine with aura. Cephalalgia 24(7):564–575
34. Manzoni GC, Farina S, Lanfranchi M, Solari A (1985) Classic migraine–clinical findings in 164 patients. Eur Neurol 24(3):163–169
35. Burke MJ, Joutsa J, Cohen AL, Soussand L, Cooke D, Burstein R, Fox MD (2020) Mapping migraine to a common brain network. Brain 143(2):541–553
36. Silvestro M, Tessitore A, Di Nardo F et al (2022) Functional connectivity changes in complex migraine aura: beyond the visual network. Eur J Neurol 29(1):295–304
37. Huang J, Zong X, Wilkins A, Jenkins B, Bozoki A, Cao Y (2011) fMRI evidence that precision ophthalmic tints reduce cortical hyperactivation in migraine. Cephalalgia 31(8):925–936
38. Schaeffer S, Iadecola C (2021) Revisiting the neurovascular unit. Nat Neurosci 24(9):1198–1209
39. Han K, Min J, Lee M et al (2019) Neurovascular coupling under chronic stress is modified by altered GABAergic Interneuron activity. J Neurosci 39(50):10081–10095
40. Fabjan A, Zaletel M, Žvan B (2015) Is there a persistent dysfunction of neurovascular coupling in migraine? Biomed Res Int 2015:574186
41. Al-Khazali HM, Ashina H, Wiggers A et al (2023) Calcitonin gene-related peptide causes migraine aura. J Headache Pain 24(1):124. https://doi.org/10.1186/s10194-023-01656-4
42. Kim KJ, Diaz R, Iddings J, J. A., Filosa JA (2016) Vasculo-neuronal coupling: Retrograde Vascular communication to brain neurons. J Neurosci 36(50):12624–12639
43. Billot PE, Comte A, Galliot E, Andrieu P, Bonnans V, Tatu L, Gharbi T, Moulin T, Millot JL (2011) Time course of odorant- and trigeminal-induced activation in the human brain: an event-related functional magnetic resonance imaging study. Neuroscience 189:370–376
44. Arngrim N, Hougaard A, Schytz HW et al (2019) Effect of hypoxia on BOLD fMRI response and total cerebral blood flow in migraine with aura patients. J Cereb Blood Flow Metab 39(4):680–689
45. Lei X, Wei M, Qi Y et al (2023) The patent foramen ovale may alter migraine brain activity: a pilot study of electroencephalography spectrum and functional connectivity analysis. Front Mol Neurosci 16:1133303
46. Buch D, Chabriat H (2019) Lamotrigine in the Prevention of Migraine with Aura: a narrative review. Headache 59(8):1187–1197
47. Li X, Tenebäck CC, Nahas Z et al (2004) Interleaved transcranial magnetic stimulation/functional MRI confirms that lamotrigine inhibits cortical excitability in healthy young men. Neuropsychopharmacology 29(7):1395–1407
48. Bridge H, Stagg CJ, Near J, Lau CI, Zisner A, Cader MZ (2015) Altered neurochemical coupling in the occipital cortex in migraine with visual aura. Cephalalgia 35(11):1025–1030
49. Menon V, Uddin LQ (2010) Saliency, switching, attention and control: a network model of insula function. Brain Struct Funct 214(5–6):655–667
50. Androulakis XM, Rorden C, Peterlin BL, Krebs K (2018) Modulation of salience network intranetwork resting state functional connectivity in women with chronic migraine. Cephalalgia 38(11):1731–1741
51. Wang R, Liu X, Sun C et al (2024) Altered neurovascular coupling in patients with mitochondrial myopathy, Encephalopathy, Lactic Acidosis, and Stroke-Like episodes (MELAS): a combined resting-state fMRI and arterial spin labeling study. J Magn Reson Imaging 60(1):327–336
52. Canna A, Esposito F, Tedeschi G et al (2022) Neurovascular coupling in patients with type 2 diabetes mellitus. Front Aging Neurosci 14:976340
53. Li P, Mu J, Ma X et al (2021) Neurovascular coupling dysfunction in end-stage renal disease patients related to cognitive impairment. J Cereb Blood Flow Metab 41(10):2593–2606
54. Friedman DI (2009) & De ver Dye, T. Migraine and the environment. Headache, 49(6), 941–952
55. Borsook D, Maleki N, Becerra L, McEwen B (2012) Understanding migraine through the lens of maladaptive stress responses: a model disease of allostatic load. Neuron 73(2):219–234

Publisher's note